

# A general framework for a joint calibration of VIX and VXX options

Martino Grasselli<sup>1,2</sup>, Andrea Mazzoran<sup>1</sup>, and Andrea Pallavicini<sup>3,4</sup>

<sup>1</sup>Department of Mathematics, University of Padova, Via Trieste 63 Padova 35121, Italy. Email: andreamazzoran@hotmail.it

<sup>2</sup>Devinci Research Center, Léonard de Vinci Pôle Universitaire, 92 916 Paris La Défense, France. Email: grassell@math.unipd.it

<sup>3</sup>Department of Mathematics, Imperial College, London SW7 2AZ, United Kingdom. Email: a.pallavicini@imperial.ac.uk

<sup>4</sup>Financial Engineering, Banca IMI, largo Mattioli 3 Milano 20121, Italy.

December 15, 2020

## Abstract

We analyze the VIX futures market with a focus on the exchange-traded notes written on such contracts, in particular, we investigate the VXX notes tracking the short-end part of the futures term structure. Inspired by recent developments in commodity smile modeling, we present a multi-factor stochastic local-volatility model able to jointly calibrate plain vanilla options both on VIX futures and VXX notes. We discuss numerical results on real market data by highlighting the impact of model parameters on implied volatilities.

**JEL classification codes:** C63, G13.

**AMS classification codes:** 65C05, 91G20, 91G60.

**Keywords:** Local volatility, Stochastic volatility, VIX, VIX futures, VXX.

## Contents

<b>1</b>	<b>Introduction</b>	<b>3</b>
<b>2</b>	<b>Stochastic local-volatility models</b>	<b>6</b>
<b>3</b>	<b>Smile modelling for ETP on futures strategies</b>	<b>7</b>
3.1	ETP on futures strategies . . . . .	7
3.2	Modeling the ETP smile . . . . .	8
<b>4</b>	<b>The VXX ETN strategy</b>	<b>11</b>
4.1	Definition of the ETN strategy . . . . .	12
4.2	The local correlation . . . . .	12
4.3	Model specification . . . . .	14
<b>5</b>	<b>Numerical illustration on a real data set</b>	<b>15</b>
5.1	VIX and VXX data sets . . . . .	15
5.2	Parameter sensitivities . . . . .	16
5.3	Joint fit of VIX and VXX market smiles . . . . .	19
<b>6</b>	<b>Conclusion and further developments</b>	<b>23</b>

# 1 Introduction

In recent years, it has become increasingly common to consider volatility as its own asset class. The great financial crisis accelerated the demand for volatility instruments and many different volatility products have been invented and are now available to trade, see [Sussman and Morgan \(2012\)](#). Created by the CBOE<sup>1</sup> in 1993, the VIX index is by far one of the most popular volatility instruments and it is considered as a landmark by most market players. It is calculated and disseminated on a real-time basis by the CBOE and represents the market's expectation of 30-day forward-looking volatility. Derived from the price inputs of the S&P 500 index options, it provides a measure of market risk and investors' sentiments. Investors, research analysts and portfolio managers look at VIX values as a way to measure market risk, fear and stress before they take investment decisions, this being a reason why it is also known as the "Fear Index". Indeed, when the VIX is rising, active investors will typically try to hedge their positions by taking short position on the market, while when the VIX is falling, active investors will closely watch the market to increase their long positions. During its origin, the formula that determined the VIX was tailored to S&P 100 index option prices, more precisely it was calculated as a weighted measure of the 30-day implied volatility of eight S&P 100 at-the-money put and call options, when the derivatives market had limited activity and was in growing stages. Ten years later, its calculation has been slightly revised when people started using a wider set of options based on the broader S&P 500 index, an expansion which allows for a more accurate view of investors' expectations on future market volatility. But apart from its role as a risk indicator, nowadays it is possible to directly invest in volatility as an asset class by means of VIX derivatives. Specifically, VIX became tradable via futures in 2004 and via options in 2006, hence providing market participants with the ability to trade liquid volatility products based on the VIX, see [Whaley \(2009\)](#). Since then, volumes on VIX futures and options drastically increased. For example, in 2015, the VIX became the second most traded underlying in the CBOE options market<sup>2</sup>, right after the S&P 500 itself.

As derivatives on the VIX may be inaccessible to non-institutional players, mainly due to the large notional sizes of the contracts as currently designed by the CBOE, some exchange-traded notes (ETN) on the VIX were introduced. In 2009, Barclays launched the first two ETN's on the VIX: VXX<sup>3</sup> and VXZ. The VXX ETN was the first exchange-traded product (ETP) on VIX futures, issued shortly after the inception of the VIX futures indices. The VXX is a non-securitized debt obligation, similar to a zero-coupon bond, but with a redemption value that depends on the level of the S&P 500 (SPX) VIX Short-Term Futures Total Return index (SPVXSTR). The SPVXSTR tracks the performance of a position in the nearest and second-nearest maturing VIX futures contracts, which is rebalanced daily to create a nearly constant 1-month maturity. In other words, VXX mimics the behaviour of the VIX, namely of the 30-day forward-looking volatility, using a replicable strategy based on futures on VIX. Since 2009 then, ETN's on the VIX flourished: there currently exist more than thirty of them, with several billion dollars in market caps and daily volumes (see [Alexander and Korovilas \(2013\)](#) for a comprehensive empirical

---

<sup>1</sup>See the white paper of CBOE in 2014 titled *CBOE Volatility Index*, available at <https://www.cboe.com/micro/vix/vixwhite.pdf>.

<sup>2</sup>See the white paper of CBOE in 2016 titled *CBOE holdings reports trading volume for 2015*, available at <http://ir.cboe.com/~media/Files/C/CBOE-IR-V2/press-release/2016/cboe-holdings-volume-report-december-2015.pdf>.

<sup>3</sup>See the VXX Prospectus of Barclays available at <https://www.ipathetn.com/US/16/en/instruments.app?searchType=text&dataType=html&searchTerm=VXX>

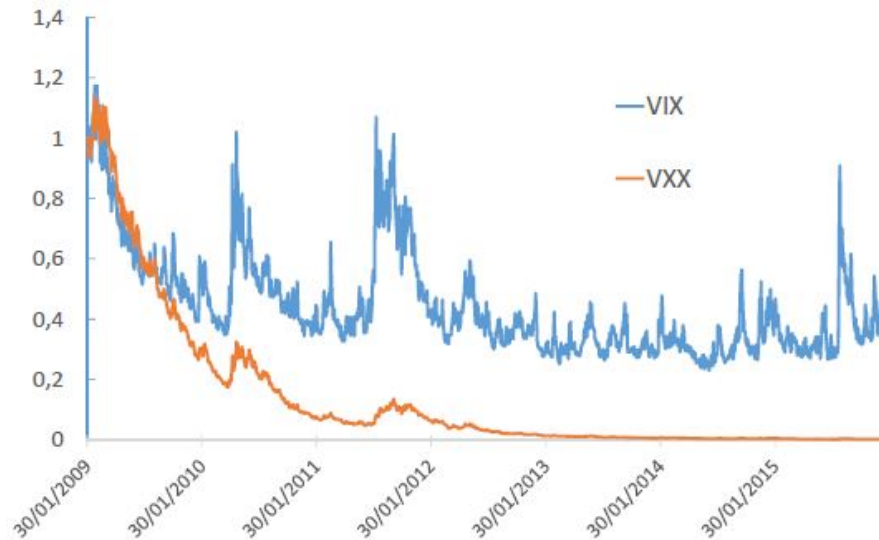


Figure 1: Prices in dollars of VIX (in blue) and VXX (in red), normalized to 1 on 30 January 2009.

study on VIX ETN's).

One of the main reasons for the high interest in these products is that VIX derivative positions can be used to provide protection against the risks inherent in the S&P500 index, especially in downturns. At the same time, VIX derivatives allow investors to achieve exposure to S&P500 volatility more cheaply than by using traditional derivatives on this broad stock market index. However, the poor performance of some of these derivative assets during decreasing volatility periods has raised some concerns about their risks among market players and regulators<sup>4</sup>. Even though VXX is very heavily traded, it has lost 99.84% of its value since inception and Figure 1 shows the remarkable underperformance of VXX compared to VIX. Whereas many market players use VXX as a proxy for trading VIX in a cheap manner, in the VXX Prospectus<sup>3</sup> Barclays warns VXX holders that "Your ETN is not Linked to the VIX index and the value of your ETN may be less than it would have been had your ETN been linked to the VIX Index".

In literature, attempts to model VIX can be divided in two strands: on the one hand, the consistent-pricing approach models the joint (risk-neutral) dynamics of the S&P 500 and the VIX with, most often, the aim of pricing derivatives on the two indices in a consistent manner, on the other hand, the stand-alone approach directly models the dynamics of the VIX.

In the former case, we can include the work of Cont and Kokholm (2013) and references therein, while more applications can be found in the work of Gehricke and Zhang (2018), where they propose a consistent framework for S&P 500 (modelled with a Heston-like specification) and the VIX derived from the square root of the variance swap contract. On top of that, they construct the VXX contract from the Prospectus and show that the roll yield of VIX futures drives the difference between the VXX and VIX returns on time series. More recently, in the paper of Gatheral et al. (2020), a joint calibration of SPX and VIX smile has been successfully obtained using the quadratic rough Heston

<sup>4</sup>See the white paper of Bloomberg in 2012 titled *SEC said to review Credit Suisse VIX Note* available at <https://www.bloomberg.com/news/articles/2012-03-29/sec-said-to-review-credit-suisse-vix-note>.

model, while [Guyon \(2020b\)](#) builds up a non-parametric discrete-time model that jointly and exactly calibrates to the prices of SPX options, VIX futures and VIX options. We also mention the work of [Guyon \(2020a\)](#), where the author investigates conditions for the existence of a continuous model on the S&P 500 index (SPX) that calibrates the full surface of SPX and VIX implied volatilities, and the paper of [De Marco and Henry-Labordere \(2015\)](#), where the authors bound VIX options from vanilla options and VIX futures, which leads to a new martingale optimal transport problem that they solve numerically.

In the latter case, the first stand-alone model for the VIX was proposed by Whaley, see [Whaley \(1993\)](#), where he models the spot VIX as a geometric Brownian motion, hence enabling to price options on the VIX in the Black and Scholes framework, but failing to capture the smile effect and the mean-reversion of volatility processes, which is necessary in order to fit the term structure of futures prices ([Schwert \(1990\)](#), [Pagan and Schwert \(1990\)](#) and [Schwert \(2011\)](#)). We cite also the attempt of [Drimus and Farkas \(2013\)](#) based on local volatility. Since then, numerous stand-alone models have been proposed for the VIX. We refer to [Bao et al. \(2012\)](#) and [Lin \(2013\)](#) for a detailed review on that strand of literature.

The literature on VXX is limited. To our knowledge, there are only a few theoretical studies which propose a unified framework for VIX and VXX. Existing studies on the VXX ([Bao et al. \(2012\)](#)) typically model the VXX in a stand-alone manner, which does not take into account the link between VIX and VXX. As a consequence, the loss for VXX when the VIX is in contango cannot be anticipated in such models. In the recent paper of [Gehricke and Zhang \(2020\)](#), they analyze the daily implied volatility curves of the VXX options market alone (where they consider the implied volatility as a function of the moneyness through quadratic polynomial regressions), providing a necessary benchmark for developing a VXX option pricing model.

We also mention the work of [Grasselli and Wagalath \(2020\)](#), where the authors were able to link the properties of VXX to those of the VIX in a tractable way. In particular, they quantify the systematic loss observed empirically for VXX when the VIX futures term-structure is in contango and they derive option prices, implied volatilities and skews of VXX from those of VIX in infinitesimal developments. The affine stochastic volatility model of [Grasselli and Wagalath \(2020\)](#) exploits the FFT methodology in order to price futures and options on VIX, while a Monte Carlo simulation is performed in order to compare the resulting smile on the VXX implied by the calibrated model with the one provided by real market data. The results are not completely satisfactory, which is not surprising, since the VXX can be seen as an exotic path-dependent product on VIX, so that the information regarding the smile on vanillas (on VIX) are well known to be not enough to recover the whole information concerning path dependent products (see for instance [Bergomi \(2015\)](#)).

In the present paper we leave the pure stochastic volatility model for the VIX and we introduce a stochastic local-volatility model (SLV), that is able to jointly calibrate VIX and VXX options in a consistent manner. The same methodology can be easily extended to other pairs of futures contracts and notes. SLV models are the de-facto industry standard in option pricing since they allow to join the advantages of stochastic volatility models with a good fit of plain options. They were first introduced in [Lipton \(2002\)](#), while a first efficient PDE-based calibration procedure was presented in [Ren et al. \(2007\)](#). In the present paper, since we investigate multi-factor models, we follow the calibration approach of [Guyon and Henry-Labordère \(2012\)](#), which is based on a Monte Carlo simulation. The SLV model we introduce for the VIX futures starts from the work of [Nastasi et al. \(2020\)](#), where the problem of modelling futures smiles for commodity

assets in a flexible but parsimonious way is discussed. In particular, here we investigate a multi-factor extension of such model which is tailored to describe VIX futures prices, and to allow a joint calibration of VIX and VXX plain vanilla options.

The key feature of our model is the possibility to decouple the problems of calibrating VIX plain vanilla options, which are recovered by a suitable choice of the local-volatility function, from the more complex task of calibrating the plain vanilla options on the VXX notes. We recall that in our approach the VXX notes are exotic path-dependent product written on VIX futures. We solve the second problem by introducing a local-correlation function between the factors driving the futures prices, and by properly selecting the remaining free dynamics parameters. The calibration of the local correlation function is inspired by the work of [Guyon \(2017\)](#).

The paper is organized as follows. In Section 2 we give a brief overview of SLV models, highlighting their properties and the main advantages in using these models. In Section 3, we present the general setting of our model. We start from the evolution of a general ETP and their underlying futures contracts, then we describe how to calibrate futures prices and options on futures. In Section 4 we adapt the general framework of the previous section to the case of the VXX ETN strategy. In Section 5 a calibration exercise based on real data along with numerical results and comparisons are presented, involving a joint fit and a parameters sensitivity analysis. In Section 6 we draw some conclusion and remarks.

Needless to say, the views expressed in this paper are those of the authors and do not necessarily represent the views of their institutions.

## 2 Stochastic local-volatility models

One of the main advantages of using local-volatility models (LV) is their natural modelling of plain-vanilla market volatilities. Indeed, a LV model can be calibrated with extreme precision to any given set of arbitrage-free European vanilla option prices. LV model were first introduced by [Dupire et al. \(1994\)](#) and [Derman and Kani \(1994\)](#). Although well-accepted, LV models have certain limitations, for example, they generate flattening implied forward volatilities, see [Rebonato \(1999\)](#), that may lead to a mispricing of financial products like forward-starting options.

On the other hand, stochastic volatility (SV) models, like the well known Heston model, see [Heston \(1993\)](#), are considered to be more accurate choices for pricing forward volatility sensitive derivatives, see [Gatheral \(2011\)](#). Although the SV models have desired features for pricing, they often cannot be very well calibrated to a given set of arbitrage-free European vanilla option prices. In particular, the accuracy of the Heston model for pricing short-maturity options in the equity market is typically unsatisfactory.

One possible improvement to the previous issues is considering stochastic local-volatility models (SLV), that take advantages of both LV and SV models properties. SLV models, going back to [Lipton \(2002\)](#), are still an intricate task, both from a theoretical as well as a practical point of view. The main advantage of using SLV models is that one can achieve both a good fit to market series data and in principle a perfect calibration to the implied volatility smiles. In such models the discounted price process  $(S_t)_{t \geq 0}$  of an asset follows the stochastic differential equation (SDE)

$$dS_t = S_t \ell(t, S_t) v_t dW_t, \quad (2.1)$$

where  $(v_t)_{t \geq 0}$  is some stochastic process taking real values, and  $\ell(t, K)$  is a sufficiently regular deterministic function, the so-called leverage function, depending on time and on

the current value of the underlying asset.  $W_t$ , as usual, is a one-dimensional Brownian motion, possibly correlated with the noise driving the process  $v$ . Obviously, SV and LV models are recovered by setting  $\ell(t, K) \equiv 1$  or  $v \equiv 1$ , respectively. At this stage, the stochastic volatility process  $(v_t)_{t \geq 0}$  can be very general and by a slight abuse of terminology we call  $(v_t)_{t \geq 0}$  stochastic volatility as in the SV model.

The leverage function  $\ell(t, K)$  is the crucial part in this model. It allows in principle to perfectly calibrate the market implied volatility surface. In order to achieve this goal,  $\ell$  needs to satisfy the following relation:

$$\ell^2(t, K) = \frac{\sigma_{\text{Dup}}^2(t, K)}{\mathbb{E}[v_t^2 | S_t = K]}, \quad (2.2)$$

where  $\sigma_{\text{Dup}}$  denotes Dupire local-volatility function, see [Dupire \(1996\)](#). The familiar reader would recognize in Equation (2.2) an application of the Markovian projection procedure, a concept originating from the celebrated Gyöngy Lemma, see [Gyöngy \(1986\)](#), whose idea basically lies in finding a diffusion which “mimics” the fixed-time marginal distributions of an Itô process.

For the derivation of Equation (2.2), we refer to [Guyon and Henry-Labordere \(2013\)](#). Notice that Equation (2.2) is an implicit equation for  $\ell$  as it is needed for the computation of  $\mathbb{E}[v_t^2 | S_t = K]$ . It is a standard thing in SLV models and this in turn means that the SDE for the price process  $(S_t)_{t \geq 0}$  is actually a McKean-Vlasov SDE, since the probability distribution of  $S_t$  enters the characteristics of the equation. Existence and uniqueness results for this equation are not obvious in principle, as the coefficients do not typically satisfy standard conditions like for instance Lipschitz continuity with respect to the so-called Wasserstein metric. In fact, deriving the set of stochastic volatility parameters for which SLV models exist uniquely, for a given market implied volatility surface, is a very challenging and still open problem. In the sequel, we will limit to investigate numerically the validity of the assumption just stated in our specific framework.

### 3 Smile modelling for ETP on futures strategies

We start this section with a wider look to study the volatility smile of a generic ETP based on futures strategies. Then, the results shown in this section will be applied to our specific VXX case in Section 4.

#### 3.1 ETP on futures strategies

We analyze an ETP based on a strategy of  $N$  futures contracts  $F_t(T)$ . If we assume that the ETP strategy itself is not collateralized and it requires a proportional fee payment  $\phi_t$ , we can write the strategy price process  $V_t$  as given by

$$\frac{dV_t}{V_t} = (r_t - \phi_t)dt + \sum_{i=1}^N \omega_t^i \frac{dF_t(T_i)}{F_t(T_i)}, \quad (3.3)$$

where  $r_t$  is the risk-free rate. Moreover, we assume that the futures contracts and the ETP are expressed in the same currency as the bank account based on  $r_t$ . The processes  $\omega_t^i$  represent the investment percentage (or weights) in the futures contracts, and they are defined by the ETP term-sheet. Notice that the weights may depend on the whole vector of futures prices. It is straightforward to extend the analysis to more general ETP strategies based on total-return or dividend-paying indices. Moreover, we can introduce securities in foreign currencies as in [Moreni and Pallavicini \(2017\)](#).



We can consider as a first example the family of S&P GSCI commodity indices. Exchange-Traded Commodity (ETC's) tracking these indices are liquid in the market, and they represent an investment in a specific commodity or commodity class. The investment is in the first nearby one-month future, but for the last five days of the contract, where a roll over procedure is implemented to sell the first nearby and to buy the second one. A second example are the volatility-based ETN's VXX and VXZ. They represent respectively an investment in short-term or in the long-term structure of VIX futures. The investment is in a portfolio of futures mimicking a rolling one-month contract. In Section 4 we will focus on the VXX case.

### 3.2 Modeling the ETP smile

We wish to jointly model the volatility smile of an ETP and of its underlying futures contracts. Indeed, market quotes for ETP plain-vanilla options can be found on the market. The main problem to solve is the fact that the price process of the ETP strategy is non-Markov, since it depends on the futures contract prices, namely the vector process  $[V_t, F_t(T_1), \dots, F_t(T_N)]$  is Markov.

We first start by modelling the marginal distribution of futures prices, then we proceed to describe the full model. The marginal distribution is modelled by following the procedure developed in [Nastasi et al. \(2020\)](#) and originally implemented for the commodity market. We consider that the futures prices  $F_t^s(T_i)$  can be modelled in term of a common process  $s_t$ , which we can identify with the price of a rolling futures contract. Futures prices are defined in term of  $s_t$  as given by

$$F_t^s(T_i) = F_0(T_i) \left( 1 - (1 - s_t) e^{-\int_t^{T_i} a(u) du} \right) \quad (3.4)$$

where  $F_0(T_i)$  are the futures prices as observed today in the market, and  $a$  is a non-negative function of time. The value of the futures at maturity times  $t$ , which are not quoted in the market, can be obtained by interpolation, but they are never used in actual calculations. The driving risk process  $s_t$  is modelled by a mean-reverting local-volatility dynamics, namely

$$ds_t = a(t) (1 - s_t) dt + \eta(t, s_t) s_t dW_t^s, \quad s_0 = 1, \quad (3.5)$$

where  $\eta$  is a positive and bounded function of time and price, to be determined by the calibration of options of futures, and  $W_t^s$  is a standard Brownian motion under the risk-neutral measure. As a consequence, the futures prices follows a local-volatility dynamics given by

$$dF_t^s(T_i) = \eta_F(t, T_i, F_t^s(T_i)) dW_t^s, \quad (3.6)$$

where we define

$$\eta_F(t, T_i, K) := \left( K - F_0(T_i) \left( 1 - e^{-\int_t^{T_i} a(u) du} \right) \right) \eta(t, k_F(t, T_i, K)), \quad (3.7)$$

$$k_F(t, T_i, K) := 1 - \left( 1 - \frac{K}{F_0(T_i)} \right) e^{\int_t^{T_i} a(u) du}. \quad (3.8)$$

Thus, plain-vanilla options on futures can be calculated as plain-vanilla options on the process  $s_t$ , which, in turn, can be easily computed by means of the Dupire equation. More precisely, given the dynamics in Equation (3.5), we have that the normalized call price

$$c(t, k) := \mathbb{E} \left[ (s_t - k)^+ \right] \quad (3.9)$$



satisfies the parabolic PDE

$$\partial_t c(t, k) = \left( -a(t) - a(t)(1 - k)\partial_k + \frac{1}{2}k^2\eta^2(t, k)\partial_k^2 \right) c(t, k), \quad (3.10)$$

with boundary conditions

$$c(t, 0) = 1, \quad c(t, \infty) = 0, \quad c(0, k) = (1 - k)^+. \quad (3.11)$$

A more detailed analysis and a proof of this (extended) Dupire equation can be found in [Nastasi et al. \(2020, Proposition 4.1\)](#). Given the prices of options on futures from the market, we can plug their corresponding normalized call prices in Equation (3.10), and then solve it for the function  $\eta$ . Then, we can compute the futures local-volatility function  $\eta_F(t, T_i, K)$ , thanks to the mapping in Equation (3.7), and eventually recover the prices of options on futures.

There is a vast literature on how to solve Equation (3.10) with the boundary conditions (3.11), here we use an implicit PDE discretization method, as usually done for solving the Dupire equation, see for example [Gatheral \(2011\)](#). We allow a mean-reversion  $a(t)$  possibly different from zero when we are calibrating the model to options on futures. On the other hand, options on the ETP spot price can be directly calibrated by a standard local-volatility model, that is without a mean-reversion term. Hence, once  $a(t)$  is chosen, we can calibrate to the market  $\eta_F(t, T_i, K)$  and  $\eta_V(t, K)$ , as previously described.

Thanks to the normalized spot dynamics (3.5), we can price all futures options by evaluating the PDE (3.10), and ETP options as well. In this way we implicitly obtain the marginal probability densities of futures prices and ETP prices.

We are now looking for the joint probability densities of futures prices, in order to be able to jointly model the dynamics of both the ETP strategy and its underlying futures. In order to do that, we need to specify a non trivial correlation structure among the futures. Notice that, for example, a one factor model based on the normalised spot dynamics, as in Equation (3.5), would not be able to produce a non-trivial final correlation among futures, see [Nastasi et al. \(2020, Section 5.1\)](#). Hence, we have to enrich our model by adding new risk factors.

We start by introducing a generic stochastic volatility dynamics for futures prices under the risk-neutral measure, as given by

$$dF_t(T_i) = \nu_t(T_i) \cdot dW_t, \quad (3.12)$$

where  $\nu_t(T_i)$  are vector processes, possibly depending on the futures price itself, and  $W_t$  is a vector of standard Brownian motions under the risk-neutral measure. The notation  $a \cdot b$  refers to the inner product between vectors  $a$  and  $b$ .

In general, we can numerically solve together Equations (3.3) and (3.12) to calculate options prices on the ETP or on the futures contracts. Our aim is at calibrating both the futures and the ETP quoted smile. In the following, we always assume that interest rates and fees are deterministic functions of time, so that we write:  $r_t := r(t)$  and  $\phi_t := \phi(t)$ . We can simplify the problem by noticing that we need only to know the marginal densities of the futures and ETP prices, so that we can focus our analysis on the Markovian projection of the dynamics (3.3) and (3.12). In this way, the model can match the marginal densities of futures prices and ETP prices predicted by the local-volatility model.

**Proposition 3.1.** *Given the dynamics (3.12) and (3.3), the Markov projections of the underlying processes  $F_t$  and  $V_t$  are given by*

$$d\tilde{F}_t(T_i) = \eta_F(t, T_i, \tilde{F}_t(T_i)) d\tilde{W}_t^i, \quad \eta_F(t, T_i, K) := \sqrt{\mathbb{E}[\|\nu_t(T_i)\|^2 \mid F_t(T_i) = K]}, \quad (3.13)$$

and

$$\frac{d\tilde{V}_t}{\tilde{V}_t} = (r_t - \phi_t) dt + \eta_V(t, \tilde{V}_t) d\tilde{W}_t^0, \quad \eta_V(t, K) := \sqrt{\mathbb{E} \left[ \sum_{i,j=1}^N \hat{\omega}_t^i \nu_t(T_i) \cdot \nu_t^T(T_j) \hat{\omega}_t^j \middle| V_t = K \right]}, \quad (3.14)$$

respectively, where  $\tilde{W}_t^0$  and  $\tilde{W}_t^i$ ,  $i = 1, \dots, N$  are scalar Brownian motions and

$$\hat{\omega}_t^i := \frac{\omega_t^i}{F_t(T_i)}. \quad (3.15)$$

The main ingredient for proving Proposition 3.1 is the Gyöngy Lemma, see Gyöngy (1986), that for the sake of clarity we recall here below.

**Lemma 3.1** (Gyöngy). *Let  $X(t)$  be given by*

$$X_t = X_0 + \int_0^t \alpha(s) ds + \int_0^t \beta(s) dW_s, \quad t \geq 0 \quad (3.16)$$

where  $W$  is a Brownian motion under some probability measure  $\mathbb{P}$ , and  $\alpha, \beta$  are adapted bounded stochastic processes such that (3.16) admits a unique solution.

If we define  $a(t, x)$ ,  $b(t, x)$  by

$$\begin{aligned} a(t, x) &= \mathbb{E}[\alpha(t) | X(t) = x] \\ b^2(t, x) &= \mathbb{E}[\beta^2(t) | X(t) = x], \end{aligned} \quad (3.17)$$

then there exists a filtered probability space  $(\tilde{\Omega}, \tilde{\mathcal{F}}, \{\tilde{\mathcal{F}}\}_{t \geq 0}, \tilde{\mathbb{P}})$  where  $\tilde{W}$  is a  $\tilde{\mathbb{P}}$ -Brownian motion, such that the SDE

$$Y_t = Y_0 + \int_0^t a(s, Y(s)) ds + \int_0^t b(s, Y(s)) d\tilde{W}_s, \quad t \geq 0 \quad (3.18)$$

admits a weak solution that has the same one-dimensional distributions as  $X$ . The process  $Y$  is called the Markovian projection of the process  $X$ .

*Proof.* (Proposition 3.1) Equation (3.13) follows from equation (3.12) and from Lemma 3.1. Dynamics (3.3) can be rewritten as

$$\frac{dV_t}{V_t} = (r_t - \phi_t) dt + \sum_{i=1}^N \omega_t^i \frac{\nu_t(T_i) \cdot dW_t}{F_t(T_i)}, \quad (3.19)$$

and applying Lemma 3.1 we get

$$\eta_V(t, K)^2 = \mathbb{E} \left[ \sum_{i,j=1}^N \frac{\omega_t^i \nu_t(T_i)}{F_t(T_i)} \cdot \frac{\nu_t^T(T_j) \omega_t^j}{F_t(T_j)} \middle| V_t = K \right], \quad (3.20)$$

while the drift part remains unaffected since both  $r_t$  and  $\phi_t$  are deterministic functions. The conclusion follows immediately.  $\square$

The functions  $\eta_F(t, T, K)$  and  $\eta_V(t, K)$  are respectively the futures and ETP local-volatility functions (we do not show the dependency of  $\eta_V(t, K)$  on all the futures maturity to lighten the notation). As already discussed previously, we can calibrate the model on plain-vanilla market quotes using the approach of Nastasi et al. (2020), that is  $\eta_F(t, T, K)$

will be calibrated using options on VIX futures and  $\eta_V(t, K)$  using options on the ETP strategy.

So far, we have preserved the marginal densities of futures prices and ETP prices, by applying the Gyöngy lemma directly on the futures and ETP dynamics, as shown in Proposition (3.1). Thus, we can calibrate our model to match the marginal densities of futures and ETP prices predicted by the local-volatility model, and in turn to match the plain vanilla option-on-futures prices and on ETP prices quoted on the market, by requiring that the process  $\nu$  satisfies Equations (3.13) and (3.14). We recall again that the local volatility for futures prices is defined in Equation (3.7), while the ETP local volatility can be recovered by using a standard local-volatility model with mean-reversion  $a = 0$ .

Hence, we have to ensure the two constraints given by the Markov projection (3.13) and (3.14) by properly choosing the vector processes  $\nu_t(T_i)$ . More precisely, we need to define a suitable dynamics for the process  $\nu_t(T_i)$  satisfying Equation (3.13) and (3.14), which in turn will enable us to preserve the calibration to plain-vanilla options. In the following, we will focus on a specific form, allowing to perform the calibration of the futures local volatility independently of the ETP dynamics. A simple way to do that is selecting the vector process  $\nu_t(T_i)$  as

$$\nu_t(T_i) \doteq \ell_F(t, T_i, F_t(T_i)) \sqrt{v_t} R(t, T_i, V_t), \quad (3.21)$$

where  $v_t$  is a scalar process independent of the futures and ETP dynamics. Here,  $\ell_F(t, T_i, K)$  is the leverage function referred to the maturity  $T_i$ , that can be computed as

$$\ell_F(t, T_i, K) = \frac{\eta_F(t, T_i, K)}{\sqrt{\mathbb{E}[v_t | F_t = K]}}, \quad (3.22)$$

where, again,  $\eta_F(t, T_i, K)$  is the futures local-volatility function. Here, the vector  $R$  plays the role of local correlation and satisfies the condition  $\|R\| = 1$ . It is the main ingredient to model the dependency between different futures and it enables us to correlate them in a natural way. In fact, Equation (3.21) satisfies by construction Equation (3.13), so that the model reprices plain-vanilla options on futures correctly. Notice that, as in standard stochastic local-volatility models, the above equation is not a definition since  $\nu_t(T_i)$  appears implicitly also on the right-hand side within the conditional law of the expectation.

We will investigate numerically in practical cases the validity of this assumption. In Section 4 we shall introduce a simple specification for  $R$  that will be enough for our purposes. Then, we shall analyze the constraint on the ETP dynamics by substituting Equation (3.21) into Equation (3.14). In other words, we are looking for conditions on  $R$  under which the model is able to reprice the ETP plain vanilla options correctly. In this way  $R$  becomes a (vector) function of the ETP price. Straightforward computations yield

$$\eta_V^2(t, K) = \sum_{i,j=1}^N R(t, T_i, K) \cdot R(t, T_j, K) \mathbb{E} \left[ v_t \hat{\omega}_t^i \hat{\omega}_t^j \ell_F(t, T_i, F_t(T_i)) \ell_F(t, T_j, F_t(T_j)) \mid V_t = K \right]. \quad (3.23)$$

In conclusion, to complete the calibration to ETP plain vanilla prices, we have to solve the above equation for an (admissible) unknown local function  $R(t, T_i, K)$ .

## 4 The VXX ETN strategy

We consider the specific case of the VIX futures and the VXX ETN strategy.

## 4.1 Definition of the ETN strategy

The VXX is defined as a strategy on the first and second nearby VIX futures, see [Gehricke and Zhang \(2018\)](#), with the following weights:

$$\omega_t^1 \doteq \frac{\alpha_1(t)F_t(T_1)}{\alpha_1(t)F_t(T_1) + \alpha_2(t)F_t(T_2)}, \quad \omega_t^2 \doteq \frac{\alpha_2(t)F_t(T_2)}{\alpha_1(t)F_t(T_1) + \alpha_2(t)F_t(T_2)}, \quad (4.24)$$

where we define

$$\alpha_1(t, T_0, T_1) := \frac{\varsigma(T_1, -1) - \varsigma(t, 1)}{\varsigma(T_1, -1) - T_0}, \quad \alpha_2(t, T_0, T_1) := 1 - \alpha_1(t, T_0, T_1), \quad (4.25)$$

with  $T_0$  being the settlement date of the futures contract just expired (the one preceding the first nearby),  $T_1$  the settlement date of the first nearby contract, and  $\varsigma(t, d)$  a calendar date shift of  $d$  business days. In this formulae we are considering  $t < T_1$ , otherwise we have to consider the following pair of future contracts.

**Remark 4.1. (Definition of the ETP weights.)** In [Grasselli and Wagalath \(2020\)](#) a slightly different definition is adopted, by using the year fraction between the second and the first nearby futures as reference time interval, instead of the year fraction between the first nearby and the previous futures contract (without calendar adjustments), leading to

$$\alpha_1(t, T_1, T_2) := \frac{T_1 - t}{T_2 - T_1}. \quad (4.26)$$

## 4.2 The local correlation

We now implement the modelling framework of the previous sections, by exploiting the structure of the local correlation vector  $R$ . A simple way to do that consists in using the following parametrization:

$$R(t, T_1, K) := [1, 0], \quad R(t, T_2, K) := [\rho(t, K), \sqrt{1 - \rho(t, K)^2}], \quad (4.27)$$

which satisfies  $\|R\| = 1$  by construction. That is, we express the dependence in terms of a local correlation coefficient  $\rho(t, K)$  that has to be determined by solving Equation (3.23).

**Remark 4.2. (Extension to higher dimensions)** The choice in Equation (4.27) relates to the case  $N = 2$ , namely two futures, but it can be easily extended to an arbitrary number  $N$ . In that case, the local correlation vector  $R(t, T_i, K)$  can be found by performing the Cholesky decomposition to the corresponding local correlation matrix.

**Proposition 4.2.** Given the parametrization in Equation (4.27), the local correlation coefficient  $\rho(t, K)$  is given by

$$\rho(t, K) = \frac{\eta_V^2(t, K) - A_1(t, K) - A_2(t, K)}{2A_{12}(t, K)}, \quad (4.28)$$

provided that  $t$  is not on a futures maturity date, where

$$\begin{aligned} A_1(t, K) &\doteq \mathbb{E} \left[ (\hat{\omega}_t^1)^2 \ell_F(t, T_1, F_t(T_1))^2 v_t \mid V_t = K \right], \\ A_2(t, K) &\doteq \mathbb{E} \left[ (\hat{\omega}_t^2)^2 \ell_F(t, T_2, F_t(T_2))^2 v_t \mid V_t = K \right], \\ A_{12}(t, K) &\doteq \mathbb{E} \left[ \hat{\omega}_t^1 \hat{\omega}_t^2 \ell_F(t, T_1, F_t(T_1)) \ell_F(t, T_2, F_t(T_2)) v_t \mid V_t = K \right], \end{aligned}$$

and where

$$\hat{\omega}_t^1 = \frac{\omega_t^1}{F_t(T_1)} = \frac{\alpha_1(t)}{\alpha_1(t)F_t(T_1) + \alpha_2(t)F_t(T_2)}, \quad \hat{\omega}_t^2 = \frac{\omega_t^2}{F_t(T_2)} = \frac{\alpha_2(t)}{\alpha_1(t)F_t(T_1) + \alpha_2(t)F_t(T_2)}. \quad (4.29)$$

We recall, once again, that the leverage function  $\ell_F(t, T_i, K)$ ,  $i = 1, 2$  is given by Equation (3.22). Notice that when  $t$  corresponds to a futures maturity date, Equation (4.28) becomes meaningless, because the weights in (4.29) vanish.

*Proof.* Exploiting the local-volatility  $\eta_V(t, K)$  in Equations (3.14) and (3.23), we get

$$\begin{aligned} \eta_V(t, K)^2 &= \mathbb{E} \left[ (\hat{\omega}_t^1)^2 \|\nu_t(T_1)\|^2 + (\hat{\omega}_t^2)^2 \|\nu_t(T_2)\|^2 + 2\hat{\omega}_t^1 \hat{\omega}_t^2 \nu_t(T_1) \cdot \nu_t^T(T_2) \mid V_t = K \right] \\ &= \mathbb{E} \left[ (\hat{\omega}_t^1)^2 \ell_F(t, T_1, F_t(T_1))^2 v_t + (\hat{\omega}_t^2)^2 \ell_F(t, T_2, F_t(T_2))^2 v_t \mid V_t = K \right] + \\ &\quad + 2\mathbb{E} \left[ \hat{\omega}_t^1 \hat{\omega}_t^2 \ell_F(t, T_1, F_t(T_1)) \sqrt{v_t} \ell_F(t, T_2, F_t(T_2)) \sqrt{v_t} \rho(t, K) \mid V_t = K \right] \\ &= \mathbb{E} \left[ (\hat{\omega}_t^1)^2 \ell_F(t, T_1, F_t(T_1))^2 v_t \mid V_t = K \right] + \mathbb{E} \left[ (\hat{\omega}_t^2)^2 \ell_F(t, T_2, F_t(T_2))^2 v_t \mid V_t = K \right] + \\ &\quad + 2\rho(t, K) \mathbb{E} \left[ \hat{\omega}_t^1 \hat{\omega}_t^2 \ell_F(t, T_1, F_t(T_1)) \ell_F(t, T_2, F_t(T_2)) v_t \mid V_t = K \right]. \end{aligned} \quad (4.30)$$

Therefore, if we define

$$\begin{aligned} A_1(t, K) &\doteq \mathbb{E} \left[ (\hat{\omega}_t^1)^2 \ell_F(t, T_1, F_t(T_1))^2 v_t \mid V_t = K \right], \\ A_2(t, K) &\doteq \mathbb{E} \left[ (\hat{\omega}_t^2)^2 \ell_F(t, T_2, F_t(T_2))^2 v_t \mid V_t = K \right], \\ A_{12}(t, K) &\doteq \mathbb{E} \left[ \hat{\omega}_t^1 \hat{\omega}_t^2 \ell_F(t, T_1, F_t(T_1)) \ell_F(t, T_2, F_t(T_2)) v_t \mid V_t = K \right], \end{aligned}$$

then, when  $t$  is not on a futures maturity date, we can obtain  $\rho(t, K)$  from Equation (4.30) and get the result.  $\square$

We can estimate the conditional expectations by means of the techniques developed in Guyon and Henry-Labordère (2012), namely approximating conditional expectations using smooth integration kernels. Thus, we can evaluate the expectation of a process  $X_t$  given a second process  $Y_t$  as

$$\mathbb{E}[X_t \mid Y_t = K] \approx \frac{\mathbb{E}[X_t \delta^\varepsilon(Y_t - K)]}{\mathbb{E}[\delta^\varepsilon(Y_t - K)]}, \quad (4.31)$$

where  $\delta^\varepsilon$  is a suitably defined mollifier of the Dirac delta depending on a smoothing coefficient  $\varepsilon$ . We can use such approximation within the Monte Carlo simulation for  $[V_t, F_t(T_1), \dots, F_t(T_N)]$  to evaluate the diffusion coefficients of the processes. Alternatively we could use the collocation method developed in Van der Stoep et al. (2014). We stress again that the existence of a solution for Equation (4.28) with the above coefficients is an open question, and, moreover, even if the solution exists, we have to check against market quotes if the chosen parametrization is able to produce a local correlation  $\rho(t, K) \in [-1, 1]$  given the plain-vanilla option prices on futures contract and ETP strategy quoted in the market.

**Remark 4.3. (Local volatility case)** *If we assume that  $v_t = 1$ , namely if we remove the stochastic volatility component, then the formulae simplify and we obtain that the options on futures can be calibrated without any further calculations, since we get*

$$\nu_t(T_i) \doteq \ell_F(t, T_i, F_t(T_i)) R(t, T_i, V_t), \quad (4.32)$$

while the local coefficients entering the calculation of the local correlation become

$$\begin{aligned} A_1(t, K) &\doteq \mathbb{E} \left[ (\hat{\omega}_t^1)^2 \eta_F(t, T_1, F_t(T_1))^2 \mid V_t = K \right], \\ A_2(t, K) &\doteq \mathbb{E} \left[ (\hat{\omega}_t^2)^2 \eta_F(t, T_2, F_t(T_2))^2 \mid V_t = K \right], \\ A_{12}(t, K) &\doteq \mathbb{E} \left[ \hat{\omega}_t^1 \hat{\omega}_t^2 \eta_F(t, T_1, F_t(T_1)) \eta_F(t, T_2, F_t(T_2)) \mid V_t = K \right]. \end{aligned}$$

Indeed, in this particular case, the leverage function  $\ell_F(t, T_i, K)$  reduces to the local-volatility function  $\eta_F(t, T_i, K)$ .

**Remark 4.4. (VXZ strategy)** *The above reasoning can be extended to the VXZ ETN strategy where four future contracts in the long part of the futures term structure are considered, in a similar way as the VXX is considering the short term, although this time we need to model a larger local correlation matrix.*

### 4.3 Model specification

We start from the stochastic local-volatility dynamics for the futures defined in Section 3, namely

$$dF_t(T_i) = \ell_F(t, T_i, F_t(T_i)) \sqrt{v_t} \cdot dW_t, \quad (4.33)$$

where the stochastic volatility component  $v_t$  follows a simple one-dimensional CIR process, namely

$$dv_t = \kappa(\theta - v_t) dt + \xi \sqrt{v_t} dZ_t, \quad (4.34)$$

with initial condition  $v(0) = v_0$  and where  $\kappa$  is the speed of the mean-reversion of the variance,  $\theta$  is the long-run average variance,  $\xi$  is the volatility-of-volatility parameter and  $\rho^v$  is the correlation between  $W$  and  $Z$ . For the sake of simplicity, we assume the same Brownian motion  $Z_t$  for the volatility of each futures  $F_t(T_i)$ ,  $i = 1, \dots, N$ , so we basically assume that all futures share the (common stochastic volatility) CIR factor  $v_t$ .

We describe the (static) correlation structure across futures dynamics by means of a positive semi-definite matrix  $\Sigma_W \in \mathbb{R}^{N \times N}$ , where  $N$  refers to the number of futures. Therefore, the correlation structure for the tuple of all the Brownian factors  $(W_t, Z_t)$  takes the following form:

$$\Sigma_{W,Z} = \begin{pmatrix} \Sigma_W & \rho_{WZ}^T \\ \rho_{WZ} & 1 \end{pmatrix} \in \mathbb{R}^{(N+1) \times (N+1)}, \quad \Sigma_W \in \mathbb{R}^{N \times N}, \quad \rho_{WZ} \in \mathbb{R}^{1 \times N}, \quad (4.35)$$

where  $\rho_{WZ} = (\rho^v, \dots, \rho^v)$  is the correlation between the Brownian motions  $W$  driving the futures and the noise  $Z$  driving the (common) stochastic volatility component  $v$ , so that the components of the vector  $\rho_{WZ}$  are all equal to the constant  $\rho^v$ .

The parameter  $\rho^v$  should be chosen in order to ensure the positive semi-definiteness of the correlation matrix  $\Sigma_{W,Z}$ . For example, in the case  $N = 2$  and  $W_1$  independent of  $W_2$ , it turns out that the parameter  $\rho^v$  needs to belong to the interval  $[-1/\sqrt{2}, 1/\sqrt{2}]$ .

VIX futures call options		
Maturities	Number of options	Strikes range (min – max)
$T_1$ : November 20, 2019	40	10 – 80
$T_2$ : December 18, 2019	40	10 – 80
$T_3$ : January 22, 2020	35	10 – 80
$T_4$ : February 19, 2020	35	10 – 80

Table 1: VIX futures call options data set as on  $T_0$ : November 7, 2019.

VXX call options		
Maturities	Number of options	Strikes range (min – max)
$T_1$ : November 20, 2019	65	8 – 60
$T_2$ : December 18, 2019	59	2 – 60
$T_3$ : January 22, 2020	53	10 – 90

Table 2: VXX call options data set as on  $T_0$ : November 7, 2019.

**Remark 4.5. (Extension to a multi-factor stochastic-volatility framework)** *Our one-factor specification for the stochastic volatility turns out to be enough for our purposes, though, of course, it is not difficult to generalise our model to a multi-factor stochastic volatility framework. What is more, this apparently more general choice does not lead to better results in the quality of the fit, up to our numerical experience.*

## 5 Numerical illustration on a real data set

In this section we perform a numerical exercise, based on real data quoted by the market for options on the VIX futures and the VXX ETN strategy, where we provide a set of admissible parameters, that is leading to an admissible local correlation vector in Equation (4.28) satisfying  $\rho(t, K) \in [-1, 1]$ . In this way we build up a coherent framework that correctly reprices plain vanilla options on futures contract and VXX strategy quoted in the market. We underline that the set of parameters we are going to find does not necessarily represent the optimal choice, namely we are just providing an admissible framework, not a full calibration. We leave for future research the complete exploration of this issue.

### 5.1 VIX and VXX data sets

We test our model against a set of three maturities for VXX call options with a corresponding set of four maturities for VIX futures call options. All data were downloaded by Bloomberg on November 7, 2019. Table 1 (resp. Table 2) describes the features of the VIX (resp. VXX) options data set.

The different maturities of VIX and VXX options as on November 7, 2019 involved in the numerical exercise are described in Figure 2. The values of VIX futures and VXX spot price, as observed in the market, are shown in Table 3, while we show in Figure 3 (resp. Figure 4) the bid, mid and ask market quotes for call options written on VIX (resp. VXX futures), for the four (resp. three) maturities of the data set.

An additional difficulty comes from the peculiar nature of the VIX-VXX options market data. In general, one can calibrate on market quotes or choose to implement a smoothing technique, like the widely-used SVI parametrization of the implied volatility smile, see Gatheral and Jacquier (2014) and the references therein. With this method, we are



Futures and Spot prices	Market Value	Maturities
$F_0(T_1)$	14.60	$T_1$ : November 20, 2019
$F_0(T_2)$	16.15	$T_2$ : December 18, 2019
$F_0(T_3)$	17.45	$T_3$ : January 22, 2020
$F_0(T_4)$	18.15	$T_4$ : February 19, 2020
Spot $V_0$	19.22	$T_0$ : November 7, 2019

Table 3: Market values of VIX futures  $F_0(T_1), \dots, F_0(T_4)$  and of the VXX spot  $V_0$  as on  $T_0$  (November 7, 2019).

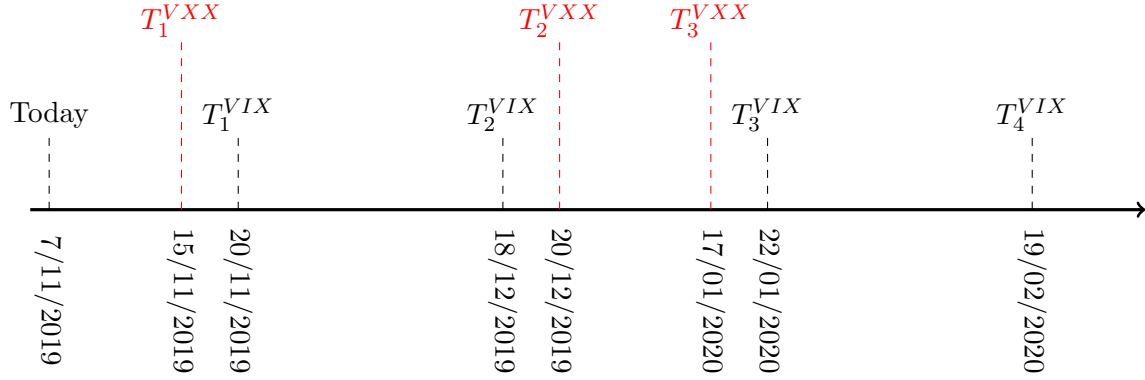


Figure 2: Maturities of options on VIX futures and VXX as on November 7, 2019 in our data set.  $T_i^{VIX}, i = 1, \dots, 4$  (resp.  $T_j^{VXX}, j = 1, \dots, 3$ ) refer to VIX futures (resp. VXX) options maturities.

guaranteed that the interpolation is arbitrage free. We applied the SVI methodology to some market quotes of VIX and VXX Call and Put options, as on May 24, 2019. Figure 5 shows that VIX market tends to be more irregular for shorter maturities, where a SVI application seems to be more needed, while it tends to be more regular as the maturities go further. On the other hand, the VXX option market seems to be more balanced overall, as Figure 6 suggests, so the SVI smoothing is not really necessary.

## 5.2 Parameter sensitivities

In this subsection, we perform a sensitivity analysis that will highlight the impact of the model parameters on the VXX smiles. The aim of this analysis is to find a range of parameters that guarantees a good fit to the VXX market smile, while maintaining the fit on the VIX market smile. Then we test if these parameters generate a local correlation  $\rho(t, K) \in [-1, 1]$ , by solving Equation (4.28). More precisely, we let each parameter vary while keeping the others frozen. In this way, we can check the overall impact of each parameter on the shape of the VXX smile. This will give us an insight on the set of reasonable parameters that can generate a good fit, provided that the local correlation in Equation (4.28) is admissible.

We shall investigate the impact of the mean-reversion speed  $a$ , the correlation between futures,  $\rho_{W_i, W_j}, i, j = 1, \dots, 4$ , the volatility-of-volatility  $\xi$  and the correlation  $\rho^v$  between futures and their (common) volatility factor  $v$ . Concerning the stochastic volatility component  $v$ , we will provide an admissible choice for the parameters  $\kappa, \theta$  and  $v_0$ , such that the Feller condition holds and the local correlation  $\rho(t, K)$  always remains in the interval  $[-1, 1]$ , without performing a sensitivity analysis, as it turns out that they do not play an



Figure 3: Bid, mid and ask market quotes for VIX futures call options, as on November 7, 2019, for the four maturities in the data set: November 20, 2019, December 18, 2019, January 22, 2020 and February 19, 2020, from the top left corner going clockwise.

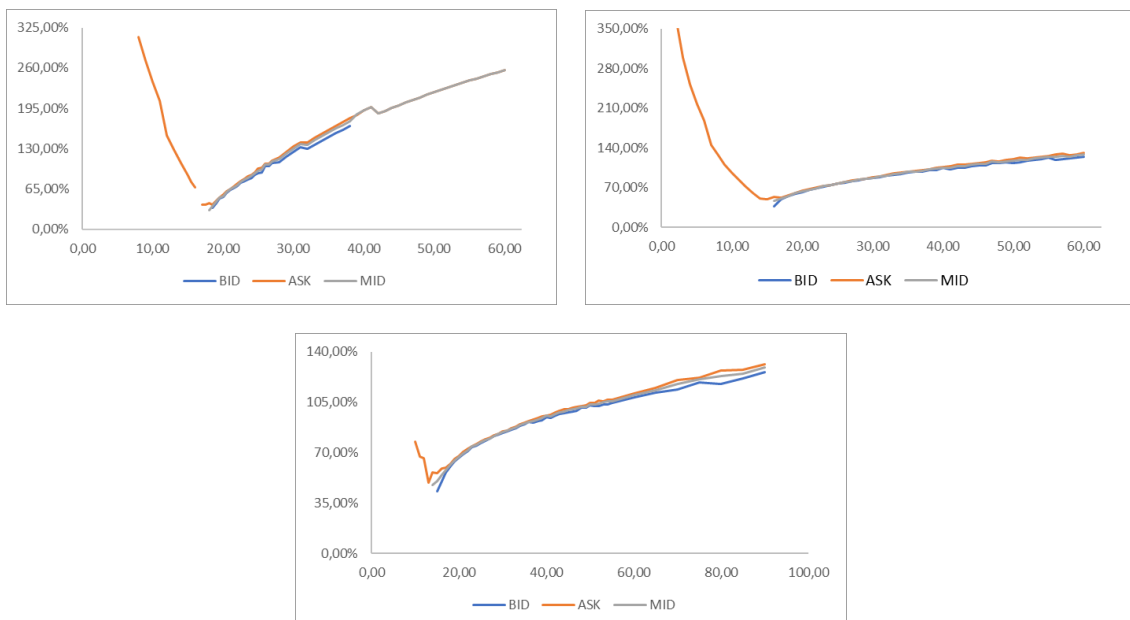


Figure 4: Bid, mid and ask market quotes for VXX call options, as on November 7, 2019, for the three maturities in the data set: November 15, 2019, December 20, 2019 and January 17, 2020, from the top to the bottom.

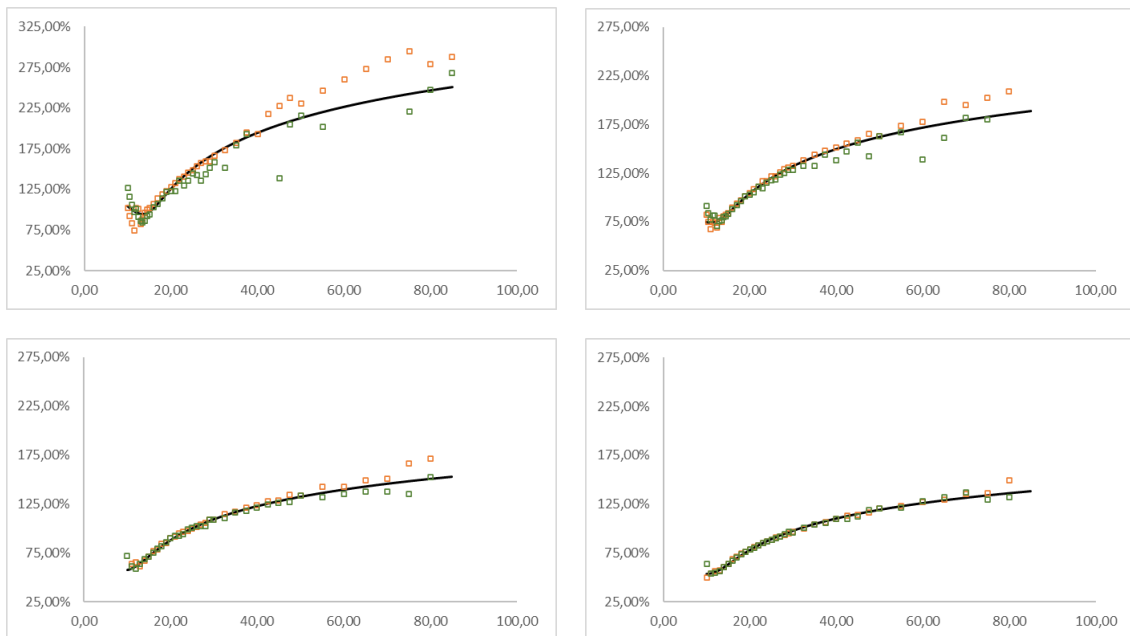


Figure 5: SVI on VIX options: continuous black lines are SVI volatility smiles . Orange squares are Call market quotes, while the green squares Put market quotes. From the top-left corner, as on May 24, 2019, pictures refer in 2019 to June 19, July 17, August 21, and September 18, respectively.

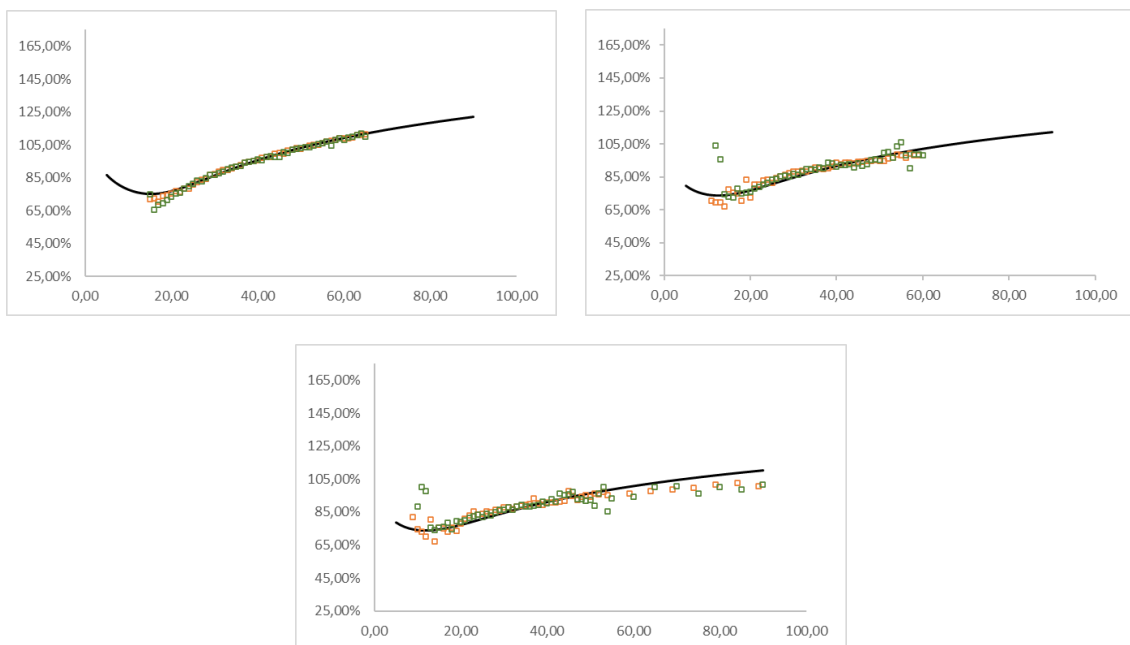


Figure 6: SVI on VXX options: continuous black lines are SVI volatility smiles . Orange squares are Call market quotes, while the green squares Put market quotes. From the top-left corner, as on May 24, 2019, pictures refer in 2019 to September 20, and December 20, in 2020 to January 17, respectively.

important role in the smile modelling. As we shall see, the impact of the mean-reversion speed  $a$  plays a crucial role in order to recover the ATM model implied volatility from the VXX options market. The impact of the correlations between futures  $\rho_{W_1, W_2}$  is also significant, while the other parameters do not really affect the shape of the VXX smile.

We start by the impact of the mean-reversion  $a$ . In Figure 7, we present the impact of the mean-reversion parameter  $a$  on the VXX smile at the first maturity, namely November 15, 2019, according to Figure 2. The results are representative also for the other maturities. In order to do that, we fixed the volatility-of-volatility  $\xi = 1.1$ , the correlation between futures  $\rho_{W_1, W_2} = 0.85$  and  $\rho^v = 0.75$ . We then let the mean-reversion speed take the values  $a = 0, 2, 4, 6, 8, 9$ . Figure 7 shows the market and the model smiles with the different choices of the mean-reversion  $a$ . We get that the higher the mean-reversion, the lower the smile. Thus, in order reproduce the market ATM implied volatility level for the VXX smile, we need a high mean-reversion speed, say around  $a = 8$ , according to Figure 7. The (high) value for the mean-reversion speed could seem misconceiving. However, we should keep in mind that we are jointly modelling two markets, the VIX and VXX option books, that display different peculiarities, therefore a somehow non standard level for the mean reversion seems a reasonable price to pay in order to reach our goal.

The impact of the correlation between futures  $\rho_{W_1, W_2}$  seems to play a pretty important role too in the shape of the VXX smile. To see this, we fix  $\rho^v = 0.75$ ,  $\xi = 1.1$ ,  $a = 8$  and let  $\rho_{W_1, W_2}$  varying according to  $-0.5, 0, 0.25, 0.55, 0.85$  and  $1$ . In Figure 8 we see that the impact of the correlation between futures tends to affect only the right tail of the smile, while leaving unaffected the left one.

Next we consider the impact of the volatility-of-volatility  $\xi$  and the correlation between futures and their volatilities, namely  $\rho^v$ . As we are going to see, these two parameters, especially  $\rho^v$ , seem to play a less pivotal role than the two ones already considered. We start with the volatility-of-volatility and as shown before, we keep the mean-reversion  $a = 8$  fixed,  $\rho_{W_1, W_2} = 0.85$ ,  $\rho^v = 0.75$  and let  $\xi$  varying within  $0.1$  and  $1.6$ , with a step of  $0.5$ . Figure 9 shows that the (positive) impact of the volatility-of-volatility is pretty significant only on the tails of the VXX smile (especially on the left ones).

Lastly, we check the impact of the correlation between futures and their volatilities, namely  $\rho^v$ . We fix  $\rho_{W_1, W_2} = 0.85$ ,  $\xi = 1.1$  and  $a = 8$  and let  $\rho_{F, Z}$  varying with  $0.25, 0.5$  and  $0.75$ . Figure 10 suggests that the correlations between futures and their volatilities,  $\rho_{F, Z}$  have a very limited impact on the shape of the VXX smile.

In the next subsection, we are going to build up a consistent framework in order to fix an admissible choice for all parameters that allows us to reproduce the market smiles of both VIX and VXX.

### 5.3 Joint fit of VIX and VXX market smiles

Thanks to the analysis performed in Subsection 5.2, we are now able to pick a cocktail of parameters that enables us to get a good fit to both the VIX and VXX market smiles and that leads to an admissible correlation parameter  $\rho(t, K) \in [-1, 1]$ . That is, the model gives the proper correlation we need to put in the VIX and VXX dynamics, in order to reprice correctly the corresponding options, as described in Section 4. Let us summarize the parameters that we have fixed in order to perform the joint fit.

- The mean-reversion speed used in the joint fit is  $a = 8$  (this value revealed to be the optimal trade-off in order to recover the ATM implied-volatility level for the VXX options, while keeping a good fit for the VIX market).
- The volatility-of-volatility parameter is fixed as  $\xi = 1.1$ .

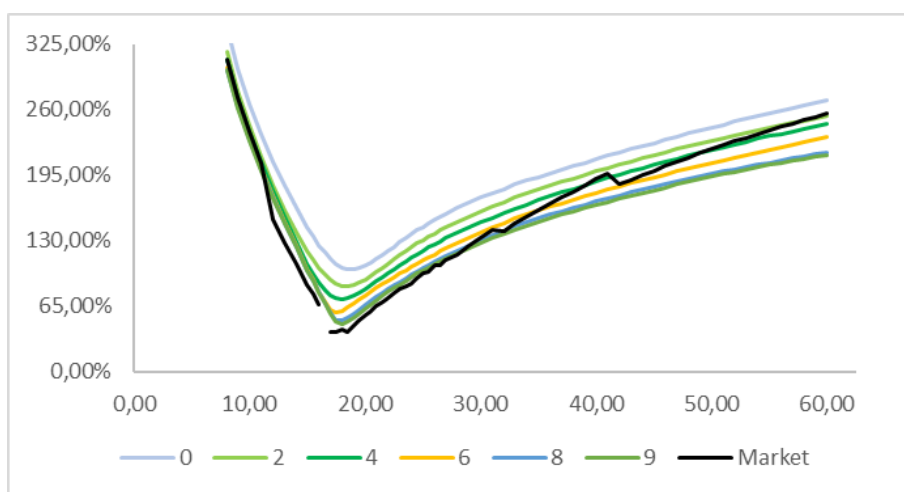


Figure 7: Impact of the mean-reversion speed  $a = 0, 2, 4, 6, 8, 9$  in the shape of the VXX smile. The other parameters are:  $\xi = 1.1$ ,  $\rho_{W_1, W_2} = 0.85$  and  $\rho^v = 0.75$ .

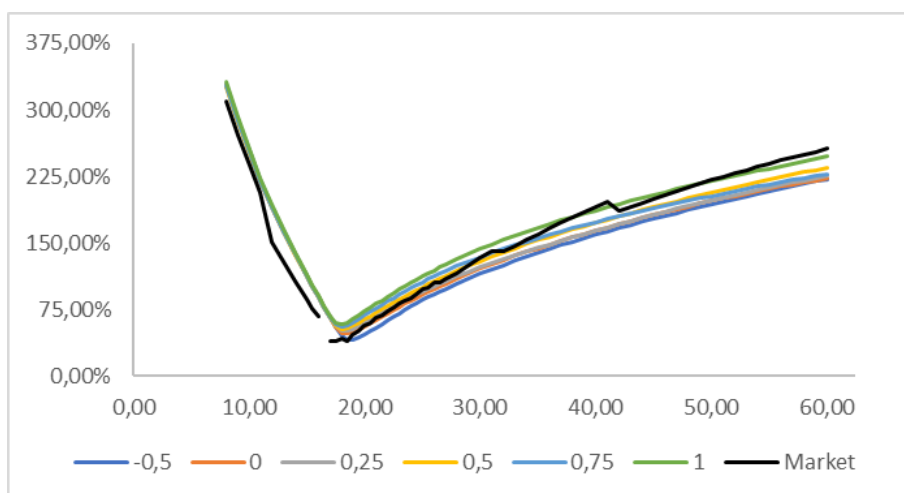


Figure 8: Impact of the correlation between futures  $\rho_{W_1, W_2} = -0.5, 0, 0.25, 0.55, 0.85, 1$  on the shape of the VXX smile. The other parameters are:  $\rho^v = 0.75$ ,  $\xi = 1.1$  and  $a = 8$ .

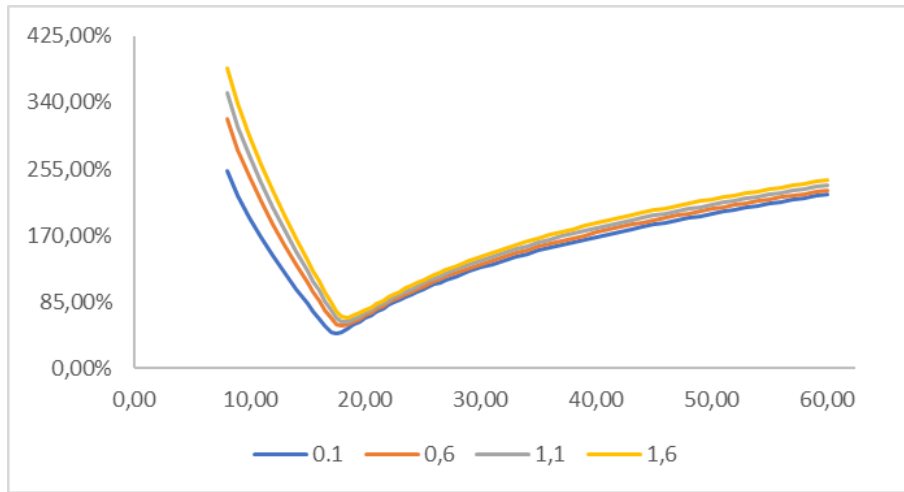


Figure 9: Impact of the volatility-of-volatility  $\xi = 0.1, 0.6, 1.1, 1.6$  in the shape of the VXX smile. The other parameters are:  $\rho_{W_1, W_2} = 0.85$ ,  $\rho^v = 0.75$  and  $a = 8$ .

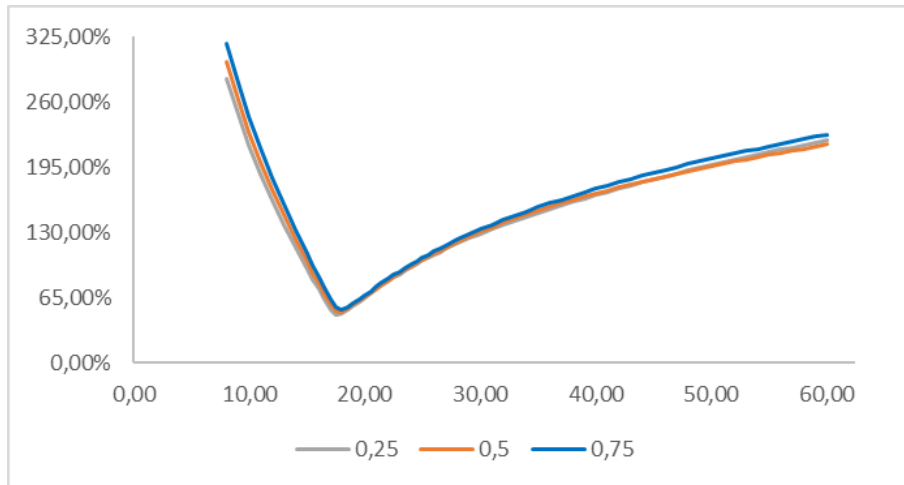


Figure 10: Impact of the correlation between futures and their volatilities  $\rho^v = 0.25, 0.5, 0.75$  on the shape of the VXX smile. The other parameters are:  $\rho_{W_1, W_2} = 0.85$ ,  $\xi = 1.1$  and  $a = 8$ .

Maturities	Strike	ASK	BID	MID	Model	Relative error
November 20, 2019	$K = 14$	1.0911	0.8042	0.9482	1.0739	0.01576
	$K = 14.5$	1.0936	0.8650	0.9792	1.0911	0.00229
	$K = 15$	1.1567	0.9297	1.0433	1.1392	0.01513
December 18, 2019	$K = 15$	0.8779	0.7519	0.8151	0.8642	0.01560
	$K = 16$	0.8995	0.7819	0.8406	0.9030	0.00389
	$K = 17$	0.8406	0.8354	0.8702	0.9170	0.09088
January 22, 2020	$K = 16$	0.7297	0.6255	0.6778	0.7263	0.00466
	$K = 17$	0.7619	0.6644	0.7131	0.7540	0.01036
	$K = 18$	0.7861	0.6911	0.7386	0.7839	0.00279
February 19, 2020	$K = 17$	0.6992	0.6020	0.6507	0.6896	0.01372
	$K = 18$	0.7157	0.6361	0.6759	0.7103	0.00754
	$K = 19$	0.7425	0.6513	0.6969	0.7360	0.00875

Table 4: Implied volatility comparison between market quotes as on November 7, 2019 and the implied volatility obtained via our SLV models for VIX call options, for the four maturities and around ATM, according to Table 3.

- The (static) correlation structure between the Brownian motions driving the VIX futures and the parameters describing the leverages, namely the correlation between futures and their common stochastic volatility CIR process, are given by the following correlation matrix between futures their volatilities: the positions  $(i, j)$ ,  $i = 1, \dots, 4$ ,  $j = 1, \dots, 4$ ,  $i < j$  represent the correlation between futures,  $\rho_{W_i, W_j}$ , while the positions  $(i, 5)$ ,  $i = 1, \dots, 4$  represent the correlation between futures and their volatilities,  $\rho^v$ .

$$\Sigma_{W,Z} = \begin{pmatrix} W_1 & W_2 & W_3 & W_4 & Z \\ 1 & 0.85 & 0.85 & 0.85 & 0.75 \\ * & 1 & 0.85 & 0.85 & 0.75 \\ * & * & 1 & 0.85 & 0.75 \\ * & * & * & 1 & 0.75 \\ * & * & * & * & 1 \end{pmatrix} \begin{matrix} W_1 \\ W_2 \\ W_3 \\ W_4 \\ Z \end{matrix}$$

- The remaining parameters used in the CIR-like volatility process are chosen by taking into account the non-violation of the Feller condition. The complete parameter list, where we repeat the entry already set for sake of clarity, is given by:

$$\kappa = 2.5, \theta = 2.5, \xi = 1.1, v_0 = 1, \rho^v = 0.75$$

We have now all the ingredients to perform the joint calibration of the implied volatilities of call options on VIX and VXX for different strikes and maturities around the ATM via the SLV method described previously which employs a Monte Carlo simulation with  $5 \cdot 10^5$  paths. In Table 4 (resp. Table 5) we show the model implied volatilities on VIX (resp. VXX) around ATM (according to Table 3), that are generated by the SLV model, and the market ones, with the relative errors.

In Figure 11 (resp. Figure 12) we show the whole implied volatilities for all strikes obtained by our SLV model and the market volatilities of VIX futures (resp. VXX) call options. Some remarks are in order: first, we calibrated on ask option quotes as they were more regular and complete, namely we considered real quotes instead of e.g. SVI interpolations. In fact, ask quotes are much more informative on the VXX market, according to



Maturities	Strike	BID	ASK	MID	Model	Relative error
November 15, 2019	$K = 19$	0.4254	0.4602	0.4429	0.4602	$\sim 0$
	$K = 19.5$	0.5027	0.5111	0.5070	0.5030	0.01584
	$K = 20$	0.5212	0.5633	0.5394	0.5473	0.02840
December 20, 2019	$K = 19$	0.6002	0.6078	0.6040	0.6050	0.00461
	$K = 19.5$	-	-	-	0.6154	-
	$K = 20$	0.6267	0.6455	0.6361	0.6329	0.01951
January 17, 2020	$K = 19$	0.6378	0.6528	0.6453	0.6450	0.01194
	$K = 19.5$	-	-	-	0.6514	-
	$K = 20$	0.6649	0.6796	0.6723	0.6735	0.00838

Table 5: Implied volatility comparison between market quotes as on November 7, 2019 and the implied volatility obtained via our SLV models for VXX call options, for the three maturities and around ATM, according to Table 3.

Figure 4. Despite the irregular shape of the market VXX smiles, the fit is overall good and even remarkably good for the VIX smiles. Recall that this market is quite irregular, with large bid-ask spreads, according to Figure 3. This means that our SLV model reproduces VIX and VXX smiles that fall within the market bid-ask spreads even after a perturbation of (some of) the parameters, according to the sensitivity analysis performed in the previous subsection. What is more, our parameters specification leads to an admissible local correlation vector  $\rho(t, K)$  that falls in the interval  $[-1, 1]$ , as required in Proposition 4.2.

## 6 Conclusion and further developments

In this paper, we have presented a general framework for a calibration of Exchange-Traded Products (ETP's) based on futures strategies. In a numerical simulation based on real data we have considered as an example of ETP the VXX ETN, which is a strategy on the nearest and second-nearest maturing VIX futures contracts. The main ingredient to achieve our goal was a full stochastic local-volatility model that can be calibrated on a book of options on a general ETP and its underlying futures contracts in a parsimonious manner.

A parameters sensitivity analysis allowed us to fix suitable values for the model parameters in order to fit the smile of the VIX and VXX ETN, with a good level of accuracy. Moreover, our specification led to an admissible local correlation function that justifies the consistency of the whole procedure. The implementation of a full calibration algorithm (in order to find the optimal value of all model parameters) based on neural networks techniques is currently under investigation. The methodology proposed has been applied to the case of VIX futures and VXX ETN, but the framework is flexible enough to tackle also more general ETP's.

Last but not least, the model is based on a simple diffusive dynamics for the VIX and it can be easily extended in order to include jumps, regime switching and other features that could be required for describing the stylized facts of this market.

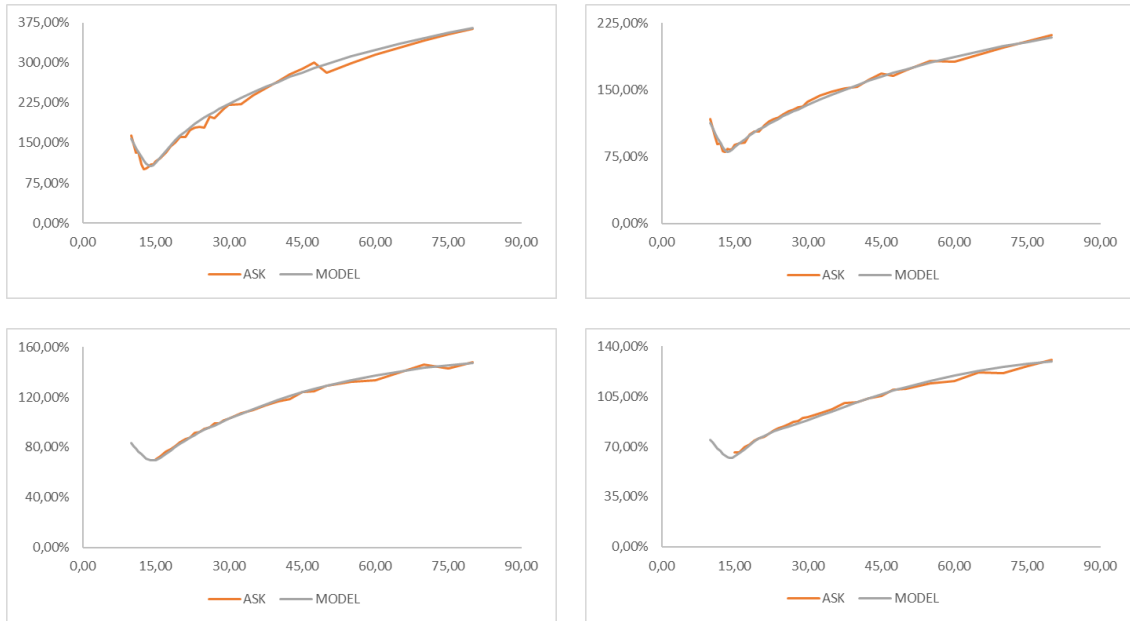


Figure 11: VIX futures model implied volatility against ask VIX call options market quotes, as on November 7, 2019, for the four maturities November 20, 2019, December 18, 2019, January 22, 2020 and February 19, 2020, from the top left corner going clockwise.

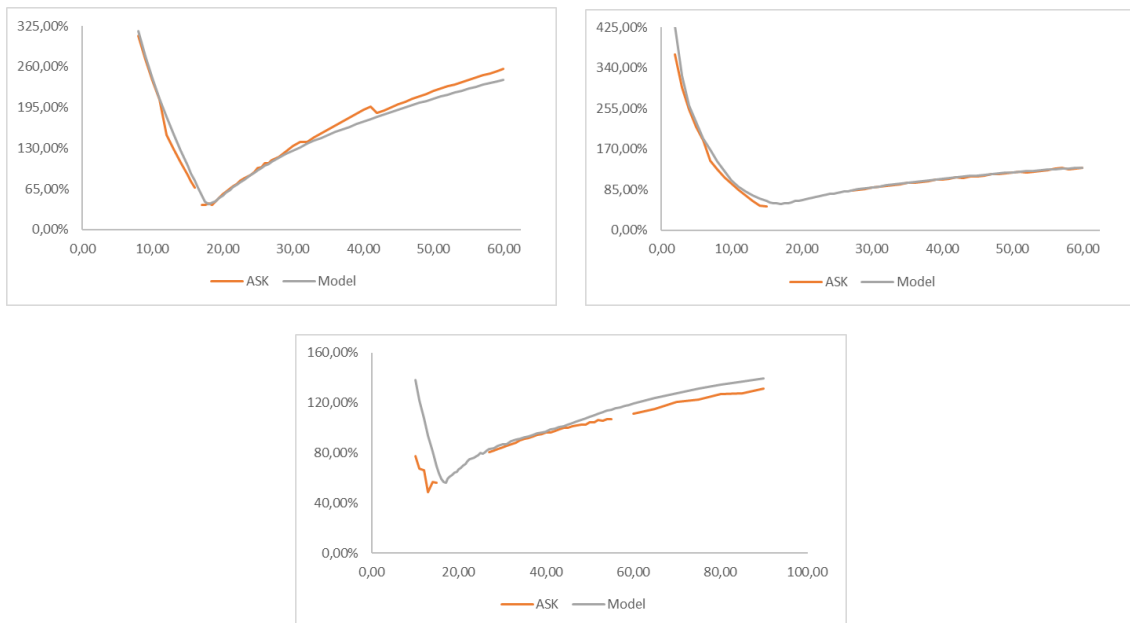


Figure 12: VXX model implied volatility against ask VXX call options market quotes, as on November 7, 2019, for the three maturities November 15, 2019, December 20, 2019 and January 17, 2020, from the top to the bottom.

## References

- Alexander, C. and Korovilas, D. (2013). Volatility exchange-traded notes: curse or cure? *The Journal of Alternative Investments*, 16(2):52–70.
- Bao, Q., Li, S., and Gong, D. (2012). Pricing VXX option with default risk and positive volatility skew. *European Journal of Operational Research*, 223(1):246–255.
- Bergomi, L. (2015). *Stochastic volatility modeling*. CRC press.
- Cont, R. and Kokholm, T. (2013). A consistent pricing model for index options and volatility derivatives. *Mathematical Finance: An International Journal of Mathematics, Statistics and Financial Economics*, 23(2):248–274.
- De Marco, S. and Henry-Labordere, P. (2015). Linking vanillas and vix options: a constrained martingale optimal transport problem. *SIAM Journal on Financial Mathematics*, 6(1):1171–1194.
- Derman, E. and Kani, I. (1994). Riding on a smile. *Risk*, 7(2):32–39.
- Drimus, G. and Farkas, W. (2013). Local volatility of volatility for the VIX market. *Review of Derivatives Research*, 3(16):267–293.
- Dupire, B. (1996). A unified theory of volatility. *Derivatives pricing: The classic collection*, pages 185–196.
- Dupire, B. et al. (1994). Pricing with a smile. *Risk*, 7(1):18–20.
- Gatheral, J. (2011). *The volatility surface: a practitioner’s guide*, volume 357. John Wiley & Sons.
- Gatheral, J. and Jacquier, A. (2014). Arbitrage-free svi volatility surfaces. *Quantitative Finance*, 14(1):59–71.
- Gatheral, J., Jusselin, P., and Rosenbaum, M. (2020). The quadratic rough heston model and the joint s&p 500/vix smile calibration problem. *arXiv preprint arXiv:2001.01789*.
- Gehricke, S. A. and Zhang, J. E. (2018). Modeling VXX. *Journal of Futures Markets*, 38(8):958–976.
- Gehricke, S. A. and Zhang, J. E. (2020). The implied volatility smirk in the VXX options market. *Applied Economics*, 52(8):769–788.
- Grasselli, M. and Wagalath, L. (2020). VIX vs VXX: A Joint Analytical Framework. *International Journal of Theoretical and Applied Finance*, 23(5):1–39.
- Guyon, J. (2017). Calibration of local correlation models to basket smiles. *Journal of Computational Finance*, 21(1):1–51.
- Guyon, J. (2020a). Inversion of convex ordering in the VIX market. *Quantitative Finance*, 20(10):1597–1623.
- Guyon, J. (2020b). The joint S&P 500/VIX smile calibration puzzle solved. *Risk*, April.
- Guyon, J. and Henry-Labordère, P. (2012). Being particular about calibration. *Risk*, 25(1):88–93.

- Guyon, J. and Henry-Labordere, P. (2013). *Nonlinear option pricing*. CRC Press.
- Gyöngy, I. (1986). Mimicking the one-dimensional marginal distributions of processes having an itô differential. *Probability theory and related fields*, 71(4):501–516.
- Heston, S. L. (1993). A closed-form solution for options with stochastic volatility with applications to bond and currency options. *The review of financial studies*, 6(2):327–343.
- Lin, Y.-N. (2013). VIX option pricing and CBOE VIX Term Structure: A new methodology for volatility derivatives valuation. *Journal of Banking & Finance*, 37(11):4432–4446.
- Lipton, A. (2002). The vol smile problem. *Risk Magazine*, 15:61–65.
- Moreni, N. and Pallavicini, A. (2017). Derivative pricing with collateralization and fx market dislocations. *International Journal of Theoretical and Applied Finance*, 20(6):1–27.
- Nastasi, E., Pallavicini, A., and Sartorelli, G. (2020). Smile modeling in commodity markets. *International Journal of Theoretical and Applied Finance*, 23(3):1–28.
- Pagan, A. R. and Schwert, G. W. (1990). Alternative models for conditional stock volatility. *Journal of econometrics*, 45(1-2):267–290.
- Rebonato, R. (1999). *Volatility and correlation: In the pricing of equity, FX and interest-rate options*. John Wiley & Sons.
- Ren, Y., Madan, D., and Qian Qian, M. (2007). Calibrating and pricing with embedded local volatility models. *Risk Magazine*, 20(9):138–143.
- Schwert, G. W. (1990). Stock returns and real activity: A century of evidence. *The Journal of Finance*, 45(4):1237–1257.
- Schwert, G. W. (2011). Stock volatility during the recent financial crisis. *European Financial Management*, 17(5):789–805.
- Sussman, A. and Morgan, C. (2012). Risk measurement on demand: Complexity, volatility and regulatory uncertainty. *TABB Group Research*.
- Van der Stoep, A. W., Grzelak, L. A., and Oosterlee, C. W. (2014). The heston stochastic-local volatility model: efficient monte carlo simulation. *International Journal of Theoretical and Applied Finance*, 17(7):1–30.
- Whaley, R. E. (1993). Derivatives on market volatility: Hedging tools long overdue. *The journal of Derivatives*, 1(1):71–84.
- Whaley, R. E. (2009). Understanding the VIX. *The Journal of Portfolio Management*, 35(3):98–105.